Global analysis of Förster resonance energy transfer in live cells measured by fluorescence lifetime imaging microscopy exploiting the rise time of acceptor fluorescence

Sergey P. Laptenok,[a] Jan Willem Borst,[bcd] Katharine M. Mullen,[e] Ivo H. M. van Stokkum,[f] Antonie J. W. G. Visser[bc] and Herbert van Amerongen*[ac]

Received 23rd September 2009, Accepted 22nd March 2010
First published as an Advance Article on the web 20th May 2010
DOI: 10.1039/b919700a

A methodology is described for the quantitative determination of Förster resonance energy transfer (FRET) in live cells using the rise time of acceptor fluorescence as determined with fluorescence lifetime imaging microscopy (FLIM). An advantage of this method is that only those molecules that are involved in the energy-transfer process are monitored. This contrasts with current methods that measure either steady-state fluorescence of donor and acceptor molecules or time-resolved fluorescence of donor molecules, and thereby probe a mixture of donor molecules that are involved in FRET and those that are fluorescent but not involved in FRET. The absence of FRET can, for instance, be due to unwanted acceptor bleaching or incomplete maturing of visible proteins that should act as acceptor molecules. In addition, parameters describing the rise of acceptor fluorescence and the decay of donor fluorescence can be determined *via* simultaneous global analysis of multiple FLIM images, thereby increasing the reliability of the analysis. In the present study, plant protoplasts transfected with fusions of visible fluorescent proteins are used to illustrate the new data analysis method. It is demonstrated that the distances estimated with the present method are substantially smaller than those estimated from the average donor lifetimes, due to a fraction of non-transferring donor molecules. Software to reproduce the presented results is provided in an open-source and freely available package called "TIMP" for "The R project for Statistical Computing".

Introduction

In order to monitor protein-protein interactions in a living cell, Förster Resonance Energy Transfer (FRET) imaging techniques have been developed. There are several methods for the quantification of FRET using intensities, spectra or lifetimes.[1] Since FRET is a fluorescence quenching process, it can be measured and characterised based on the fluorescence lifetime of donor molecules.[2] Fluorescence lifetime imaging microscopy (FLIM) is a widely used imaging technique, which allows mapping of fluorescence lifetimes with (sub)-nanosecond time resolution and a diffraction-limited, spatial resolution of approximately 250 nm. Therefore, FRET phenomena measured with a FLIM setup can provide temporal and spatial information about protein dynamics and molecular interactions in cells.[3] Recently, this approach was also used in our laboratory to study processes in photosynthesis, both *in vitro*[4] and *in vivo*.[5]

For accurate and quantitative analysis of FLIM data and of FLIM-FRET data in particular, well-designed data analysis protocols are required. Significant advantages and improved accuracy in data analysis can be achieved by applying global analysis, when data from different measurements are analyzed simultaneously. Using the fact that some parameters should be invariant in different experiments significantly increases the precision of the analysis.[6] The dynamical features of a fluorescence decay are often well described by a small number of kinetic processes, for which the associated fluorescence lifetimes in all pixels have similar values, but the relative intensity values may vary from pixel to pixel.[7]

Global analysis can be used to accurately detect FRET phenomena by estimating the fluorescence lifetimes of donor molecules in the absence and presence of acceptor molecules. Shortening of the donor fluorescence lifetime is an indicator of FRET, and the difference between the donor fluorescence lifetime with and without acceptor allows quantification of the FRET efficiency. A complicating issue is the fact that

[a] *Laboratory of Biophysics, Wageningen University, Dreijenlaan 3 6703 HA Wageningen, The Netherlands. E-mail: Herbert.vanAmerongen@wur.nl; Fax: +31317482725; Tel: +31317482634*
[b] *Laboratory of Biochemistry, Wageningen University, Dreijenlaan 3 6703 HA Wageningen, The Netherlands*
[c] *Microspectroscopy Centre, Wageningen University, Dreijenlaan 3 6703 HA Wageningen, The Netherlands*
[d] *Centre for BioSystems Genomics, 6708 PB Wageningen, The Netherlands*
[e] *Ceramics Division, National Institute of Standards and Technology, Gaithersburg, 20899-8520 Maryland, The United States of America*
[f] *Department of Physics and Astronomy, Faculty of Sciences, Vrije Universiteit, Amsterdam, De Boelelaan 1081, 1081 HV Amsterdam, The Netherlands*

FRET systems are not always purely homogeneous, since they can contain a population of donor molecules that cannot transfer their excitations, either because of unwanted bleaching (photodestruction) of the acceptor molecules or because of incomplete maturation of the acceptor proteins (in the case of visible proteins).[8,9] The average donor lifetime then originates from interacting and non-interacting species. Therefore, the average donor fluorescence lifetime does not reflect the true FRET efficiency, and distances between molecules calculated based on these lifetimes are overestimated.[10] Another method of measuring FRET uses the detection of the rise time of acceptor fluorescence following donor excitation. The main advantage of this approach is that only those molecules that are involved in energy transfer[11] are monitored but so far, this approach has not been applied in fluorescence imaging techniques.

Here, a global analysis technique is described where the rise time of the acceptor fluorescence is determined after donor excitation in order to quantify FRET in live cells and multiple FLIM images are analyzed simultaneously, in order to increase the precision of the transfer rate determination. The method has been performed on plant protoplasts, which were transfected with fusions of visible fluorescent proteins and two different constructs were used. The first one was composed of Enhanced Cyan Fluorescence Protein (ECFP) linked to Enhanced Yellow Fluorescence Protein (EYFP) by thirteen amino acids and the second one of Enhanced Green Fluorescence Protein (EGFP) linked to the red fluorescent protein mCherry by six amino acids.

Experimental

FLIM

FLIM images were recorded using the setup described in detail by Borst *et al.*[12] Briefly, the instrumentation involves a Biorad Radiance 2100 MP system coupled to a Nikon TE300 inverted microscope. To obtain two-photon excitation, a Ti:Sapphire laser (Coherent Mira D900) (Coherent Inc., Santa Clara, CA) pumped by a 5W solid state laser (Coherent Verdi V5) (Coherent Inc., Santa Clara, CA) is used to generate 150-femtosecond pulses with center wavelength 860 nm and repetition rate 76 MHz. Excitation light is focused using an apochromat 60x water immersion objective lens (CFI Plan Apochromat, numerical aperture 1.2, Nikon, Tokyo, Japan). Fluorescence is detected *via* different band-pass filters using the time-correlated single photon counting technique (TCSPC) by a Hamamatsu R3809U microchannel-plate photomultiplier operated at 3.1 kV (Hamamatsu Photonics K K, Hamamatsu, Japan) coupled to a single photon counting module SPC 730 (Becker and Hickl, Berlin, Germany). For more details see ref. 13. All images are acquired with a 64 × 64 pixels frame size and analog-to-digital converter (ADC) set to 256 channels resulting in a 48-ps/channel time interval.†

† Certain commercial equipment, instruments, or materials are identified in this paper in order to specify the experimental procedure adequately. Such identification is not intended to imply recommendation or endorsement by the National Institute of Standards and Technology, nor is it intended to imply that the materials or equipment identified are necessarily the best available for the purpose.

Experimental system

cDNA fusions of EGFP (donor) linked to mCherry (acceptor) by six amino acids (GSGSGS) (EGFP-L-mCherry) and ECFP (donor) coupled to EYFP (acceptor) *via* a 13-amino acid linker (RGGGGARDPPVAT) (ECFP-L-EYFP) were constructed. The preparation of the constructs has been described more extensively by Visser *et al.*[9] Plant protoplasts were transfected as described by Aker *et al.*[14] The calculated expression levels of fluorescent proteins by using fluorescence correlation spectroscopy as described in ref. 15 show that the maximum protein concentration is in the order of 2 μM, far below the dissociation constant for dimerization of 100 μM. In connection with this observation, fluorescence cross-correlation spectroscopy indeed demonstrated that free ECFP and free EYFP do not form complexes in plant cells.[15]

FLIM images of the protoplasts were obtained by collecting fluorescence using an appropriate band-pass filter. ECFP fluorescence was detected using a 480-nm (30 nm width) band pass filter. For the detection of EYFP fluorescence a band-pass filter of 542 nm (35 nm width) was used. Images were obtained using an acquisition time of 150 s. EGFP fluorescence was detected with a 525 nm band-pass filter (50 nm width) using an acquisition time of 80 s. The fluorescence of mCherry was detected through a 590 nm band-pass filter (30 nm width) using an acquisition time of 300 s. To build up a fluorescence decay curve with a sufficient amount of counts, decay traces from nine neighboring pixels were summed up (binning factor 1). The fusion proteins could be observed both in the cytoplasm and the nucleus of the plant cell. The image size in both case studies was 15 μm × 15 μm with a pixel size of 235 nm.

Summary of FRET theory

The lifetime of a fluorophore τ is the average time that the molecule stays in the excited state after response to an excitation pulse, and is given as a function of the radiative (k_r) and non-radiative (k_{nr}) rate constants:

$$\tau = 1/(k_r + k_{nr}) \quad (1)$$

The fluorescence lifetime strongly depends on the environment of the fluorophore. It can therefore be used for probing the environment that changes under different conditions. The time-dependence of fluorescence intensity in the most simple case is described by a single exponential decay $I(t) = I_0 e^{-t/\tau}$, where I_0 is the intensity at $t = 0$.

FRET is a bimolecular process in which the excited-state energy of a donor fluorophore is non-radiatively transferred with rate constant (k_t) to a ground-state acceptor molecule by dipole–dipole interaction. The excited-state population of the system after excitation of the donor with a δ-pulse can be described by the following set of equations

$$\begin{cases} \frac{dD(t)}{dt} = -(k_d + k_t)D(t) \\ \frac{dA(t)}{dt} = D(t)k_t - A(t)k_a \end{cases} \quad (2)$$

where $D(t)$ is the concentration of the donor molecules in the excited state, $A(t)$ is the concentration of excited

acceptor molecules, k_d is the rate constant of donor-molecule de-excitation in the absence of the acceptor and it is equal to $(k_r + k_{nr})$, and k_a is the acceptor de-excitation rate constant and k_t is the rate constant of resonance energy transfer. Solving eqn (2) results in the following functions describing the decay of exited-state concentrations of the donor and acceptor as

$$\begin{aligned} D(t) &= D_0 e^{-(k_d+k_t)t} \\ A(t) &= -\frac{D_0 k_t}{k_d + k_t - k_a} e^{-(k_d+k_t)t} + \frac{D_0 k_t}{k_d + k_t - k_a} e^{-k_a t} \end{aligned} \tag{3}$$

where D_0 is the excited-state population of the donor at $t = 0$. The negative term in the expression of $A(t)$ reflects a rise component due to energy transfer from donor to acceptor with rate constant $(k_d + k_t)$. The absolute value of the ratio between negative and positive amplitudes in the ideal case, when acceptor molecules receive energy only from donor molecules *via* FRET, is equal to 1. However, in practice, this situation is almost never observed because part of the acceptor molecules is excited directly and/or some donor fluorescence is observed in the detection window of acceptor fluorescence. In this case fluorescence, detected in the acceptor channel, besides $A(t)$ from eqn (3), will contain more terms with positive amplitudes coming from directly excited acceptor molecules and/or donor molecules. Therefore the absolute value of the ratio between negative and positive amplitudes will be smaller than 1.

The lifetime of donor molecules in the presence of FRET is shorter than the lifetime of the donor in the absence of acceptor and can be calculated using

$$\tau_{da} = 1/(k_d + k_t) \tag{4}$$

As is clear from eqn (3) the rate of the rise of acceptor fluorescence is equal to the decay rate of donor fluorescence in the presence of FRET, and it can be used for estimation of the transfer rate constant as

$$k_t = k_{da} - k_d = 1/\tau_{da} - 1/\tau_d \tag{5}$$

The transfer rate (k_t) is proportional to the inverse 6th power of the distance r between donor and acceptor, which makes it an extremely sensitive parameter for obtaining distances less than 10 nm:

$$k_t = k_d(R_0/r)^6 \tag{6}$$

where R_0 is the so-called critical or Förster radius,[16] the distance between donor and acceptor, at which 50% of the donor energy is transferred to the acceptor.

In most cases a multi-exponential analysis has to be applied to describe the observed fluorescence in time, and use can be made of the average lifetime $\langle\tau\rangle^2$ which is defined as:

$$\begin{aligned} \langle\tau\rangle &= \frac{\sum_i \alpha_i \tau_i^2}{\sum_i \alpha_i \tau_i} \\ \sum_i \alpha_i &= 1 \end{aligned} \tag{7}$$

where τ_i is the lifetime of component i, and α_i is the fractional contribution of component i. Another widely used parameter is the amplitude-averaged lifetime $\langle\tau^*\rangle$ that is defined as:

$$\begin{aligned} \langle\tau^*\rangle &= \sum_i \alpha_i \tau_i \\ \sum_i \alpha_i &= 1 \end{aligned} \tag{8}$$

FLIM data analysis

For each pixel in a FLIM image, the fluorescence is measured as a function of time. Each recording of the decay in one pixel can be considered as a separate experiment. The resulting data of all pixels is stored as a matrix in which each column represents the fluorescence decay associated with a single pixel x, such that

$$\boldsymbol{\Psi} = \left[\begin{array}{c|cccc} & x_1 & x_2 & \cdots & x_n \\ \hline t_1 & \psi(t_1,x_1) & \psi(t_1,x_2) & \cdots & \psi(t_1,x_n) \\ t_2 & \psi(t_2,x_1) & \psi(t_2,x_2) & \cdots & \psi(t_2,x_n) \\ \vdots & \vdots & \vdots & \ddots & \vdots \\ t_m & \psi(t_m,x_1) & \psi(t_m,x_2) & \cdots & \psi(t_m,x_n) \end{array}\right] \tag{9}$$

where $\psi(t_i, x_j)$ is the fluorescence intensity at time t_i in pixel x_j. In practice, the fluorescence decay can often be described well as a sum of exponential decays convolved with the instrumental response function (IRF), so that the decay model for a single pixel reads

$$F(t) = \sum_i \alpha_i \exp(-t/\tau_i) \otimes g(t) \tag{10}$$

where the summation is over the number of components n_{comp} of the decay, τ_i is the lifetime of component i, α_i is the fractional contribution of component i to the fluorescence decay, $g(t)$ is the instrumental response function and $\otimes$ is the convolution operator. Often, the IRF is not represented well by a simple analytical function, and therefore it is usually measured and numerically convolved with the exponential decay model for each component. Various algorithms for numerical convolution of an exponential decay with a measured IRF can be applied. The iterative reference and scatter methods described in ref. 17–19 have been found to perform well in practice, and are implemented in the package **TIMP** for "The *R* project for statistical computing" that is used in this study.[20] The reference convolution method was also used in the present study. The instrumental response function of the FLIM setup has been obtained by using a solution of xanthione in ethanol as a reference compound which has a mono-exponential fluorescence decay kinetic with a lifetime of 14 ps.[21,22]

The assumption that the fluorescence lifetime components are spatially invariant is a crucial one for global analysis of a FLIM image, which has been justified by Verveer and co-workers.[23] Under this assumption, the matrix dataset associated with a single FLIM image $\boldsymbol{\Psi}$ is modelled as

$$\begin{aligned} \boldsymbol{\Psi} &= \mathbf{C}\mathbf{A}^T + \mathbf{Z} = \sum_{i=1}^{n_{\text{comp}}} c_i \alpha_i^T + \mathbf{Z} \\ &= \sum_{l=1}^{n_{\text{comp}}} (\exp(-t/\tau_i) \otimes g(t))\alpha_i^T + \mathbf{Z} \end{aligned} \tag{11}$$

where column i of the matrix **C** represents the time profile of component i of the fluorescence decay, and column i of the matrix **A** represents the amplitude of component i over all pixels. The free parameters of the model are the n_{comp} lifetimes τ_i and for each pixel the n_{comp} amplitude parameters describing the fluorescence decay, stacked in n_{comp} vectors α_i, each of length n_{pixel}. The stochastic component of the model is assumed to consist of an additive Gaussian noise term **Z** with the same dimensionality as the data matrix. Note that the modeled data represent non-negative counts of the number of photons detected per pixel and per time interval, to which Poissonian noise statistics apply. However, as Maus and co-workers[24] have studied in depth, using a Gaussian approximation for the Poisson noise statistics introduces negligible errors to the parameter estimates as long as the data represent mostly a sufficiently large number of counts, which is the case for the data considered here.

The parameter estimation problem associated with fitting the model for Ψ is an example of a separable nonlinear least squares optimization problem.[25] The variable projection algorithm developed by Golub and Pereyra[26] that is used here has many advantages over other techniques for separable nonlinear least squares problems, and relies on analytically eliminating the conditionally linear amplitude parameters α_i from the residual function. The applicability of variable projection for fitting FLIM data was demonstrated by a variety of simulation studies.[27] In order to use all available data to estimate the lifetimes of the fluorescence decay of the components, a global analysis model of multiple datasets has been formulated, in which the same number of fluorescence rise and decay times underlie the decay kinetics across multiple images. Each image is associated with a possibly distinct measured IRF curve. The amplitude parameters of each component of the decay were estimated per pixel. Singular Value Decomposition (SVD)[28] of the residual matrix associated with each FLIM image has been used to diagnose the fit quality and the presence of systematic errors in the data as discussed in ref. 29 and 30.

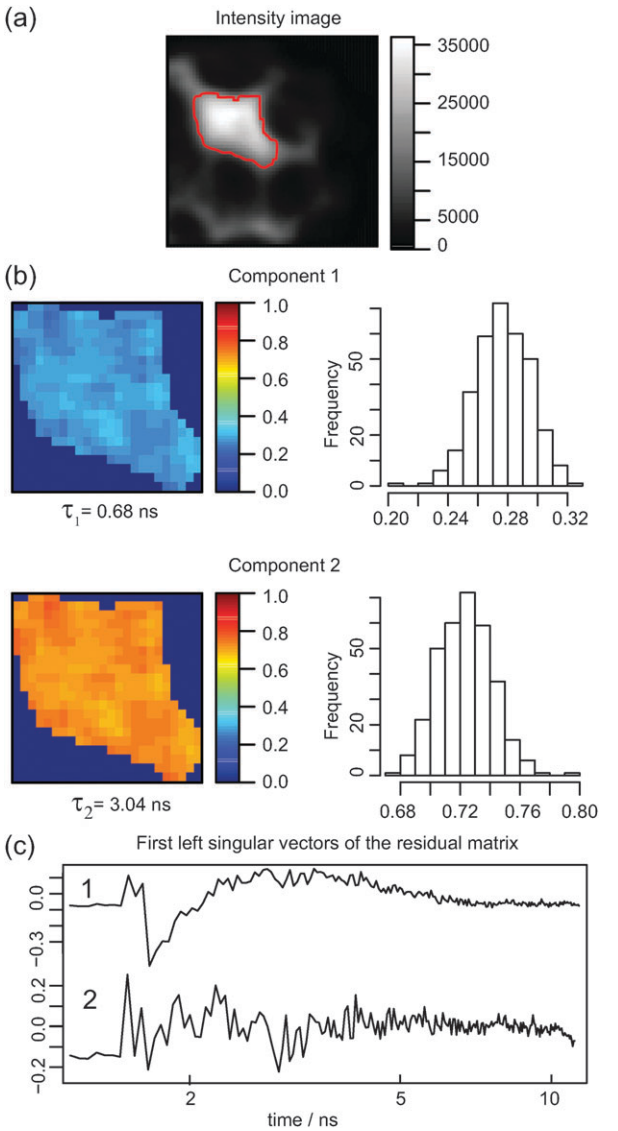

Fig. 1 Results of global analysis of ECFP fluorescence in a plant protoplast; detection at 465–495 nm (ECFP). (a) Intensity image, brightness of the pixels represents number of detected photons, (64 × 64 pixels frame size, pixel size 235 nm), red contour indicates region selected for analysis, (b) spatial distribution and histogram of the fractional distributions of the components obtained from the fit using a bi-exponential model, (c) first left singular vectors of the residuals matrix ((1) mono-exponential analysis, (2) bi-exponential analysis).

Results and discussion

ECFP-EYFP construct

ECFP is widely used as a donor molecule in FRET studies but it shows bi-exponential fluorescence dynamics even in the absence of FRET.[31,32] Fig. 1 shows the global analysis results for a plant protoplast which is transfected with ECFP molecules. In Fig. 1a the fluorescence intensity image of the plant protoplast is shown and the brightness of the pixel codes for the number of detected photons. Only the region of the nucleus was selected for further analysis. Fluorescence lifetimes were linked for all pixels within the region of interest in the analysis procedure. A bi-exponential fit leads to a satisfactory description of the data with lifetimes of 0.68 ± 0.02 ns (average contribution 27%) and 3.04 ± 0.01 ns (average contribution 73%) which results in an average lifetime calculated with eqn (7) of $\langle\tau\rangle$ = 2.85 ns, or amplitude-averaged $\langle\tau^*\rangle$ = 2.37 ns. Standard errors of the lifetime estimates are obtained from the fit as described by Mullen and co-workers.[33] The adequacy of the linear approximation of confidence intervals for the decay rate parameters in a global analysis has been thoroughly demonstrated in the past by simulation studies.[33,34] The first left singular vector of the residual matrix, which serves as an overall fit quality indicator, is given in Fig. 1c. The noise-like fluctuations around zero in case of the bi-exponential analysis show that the quality of the fit is not systematically biased. The false-color images of the analyzed area from the protoplast transfected with ECFP is shown in Fig. 1b. The color reflects the normalized amplitudes

of the components as obtained from a bi-exponential fit for each pixel in the region of interest and the frequency of the normalized amplitude is shown in the corresponding histogram. It is clear that the contributions of both components are almost the same for all pixels within the selected region. Both lifetime components correspond to populations with two different chromophore structures,[35] a quenched one (0.68 ns, 27%) and an unquenched one (3.04 ns, 73%). Chromophores of both populations can transfer excitation energy to a nearby acceptor. Therefore, in the presence of an acceptor at least a four-exponential model is needed to include both transferring and non-transferring donor molecules.[11] The estimation of four fluorescence lifetimes and the corresponding amplitudes is impossible given the typical quality of FLIM data. However, analysis of the rise of the acceptor fluorescence can be used for a more accurate determination of the FRET efficiency. The FLIM images of plant protoplasts transfected with ECFP-L-EYFP were recorded at two different detection wavelengths. First, images measured with the 542 nm band-pass filter (EYFP fluorescence detection window) were analyzed globally. The global analysis results for one representative protoplast using a bi-exponential model

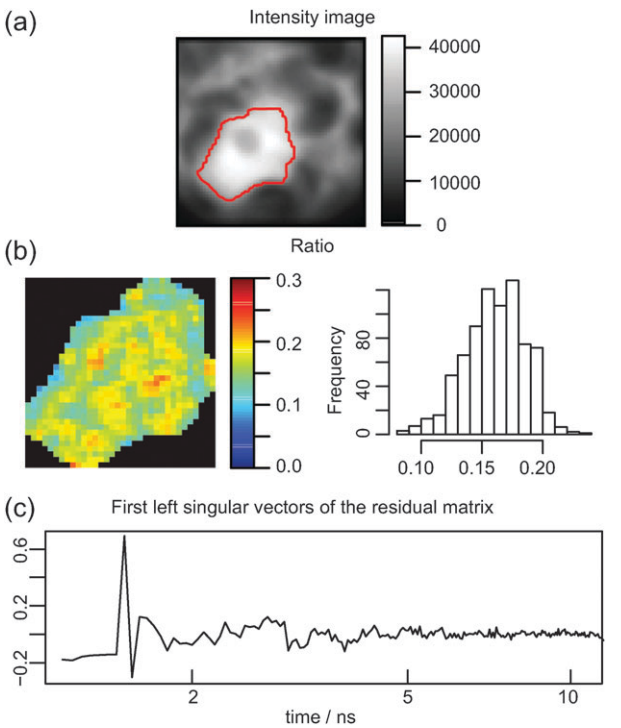

Fig. 2 Global analysis results of a representative image of a protoplast transfected with ECFP-L-EYFP detected with a 542 nm band-pass filter (EYFP fluorescence is detected). Global analysis was performed with a bi-exponential model (0.74 ns rise component and 3.01 ns decay component). (a) Fluorescence intensity image, brightness of the pixels represents number of detected photons, (64 × 64 pixels frame size, pixel size 235 nm), red contour indicates the region that is analyzed, (b) spatial distribution and histogram of the absolute value of the ratio between the negative and positive amplitudes of the fast and slow components, respectively, (c) first left singular vector of residuals.

for the fluorescence kinetics are presented in Fig. 2. It shows the presence of a rise component (*i.e.* negative amplitude) of 0.74 ± 0.1 ns and a decay component of 3.01 ± 0.05 ns. The rise time of the acceptor fluorescence corresponds to resonance energy transfer and the decay time corresponds to fluorescence of mainly EYFP.[11,36] The spatial distribution of the absolute value of the ratio between the negative and positive amplitudes is depicted in pseudo-color code in Fig. 2b. It shows a narrow distribution of this value. The ratio is smaller than 1 because of the presence of fluorescence arising both from donor molecules and from directly excited acceptor molecules. Formally speaking, it would be better to apply a three- or even four-exponential model for the description of the data, thereby accounting for the fluorescence of interacting and non-interacting donor molecules in the acceptor detection channel (crosstalk). However, the slow decay times of the acceptor and the non-transferring donor are close to each other and modeling them as a single component does not significantly influence the obtained value of the acceptor rise time. We also explicitly tested the stability of the rise time calculation in the presence of crosstalk in a previous study (see ref. 11). It should be noted that the rise time is the only parameter obtained from the acceptor channel that is needed for calculating the transfer rates and distances. The first left singular vector of the residual matrix, serving as an overall fit quality indicator in the time dimension, is given in Fig. 2c and shows the good quality of the fit.

Results of the global analysis of the images observed in the donor detection window are presented in Fig. 3. The use of a three-exponential model is necessary to obtain a good description of the data. Analysis leads to fluorescence lifetimes of 0.15 ± 0.03 ns (average contribution 26%), 0.76 ± 0.03 ns (average contribution 33%) and 2.51 ± 0.01 ns (average contribution 41%). The 0.15-ns component corresponds to auto-fluorescence; fluorescence stemming from chloroplasts using the same excitation and detection wavelength is characterized by an average lifetime of 0.17 ns (data not shown) and therefore this component was excluded from further calculations. The other two components can be assigned to interacting and non-interacting ECFP molecules, whereas one might even expect the presence of four decay components for the description of the ECFP fluorescence in the presence of FRET. Panel b of Fig. 3 shows a homogeneous and narrow spatial distribution of the fractional contribution of the components. However, there are a few regions, which show certain patterns for components 1 and 2 that mainly represent differences in the amount of auto-fluorescence.

In order to increase the precision of the fluorescence lifetime estimates and to reduce the error margins for lifetime estimates, global analysis of the FLIM images measured in both detection windows was performed. Results of the global analysis of different images, measured at both detection windows, are shown in Fig. 4 (1—detection of donor fluorescence, 2—detection of acceptor fluorescence). Representative traces with estimated lifetimes for both detection windows are given in Fig. 4e. The analysis was performed by applying a bi-exponential model for the acceptor detection window and a three-exponential model for the donor detection window. The FRET component was linked between all images and

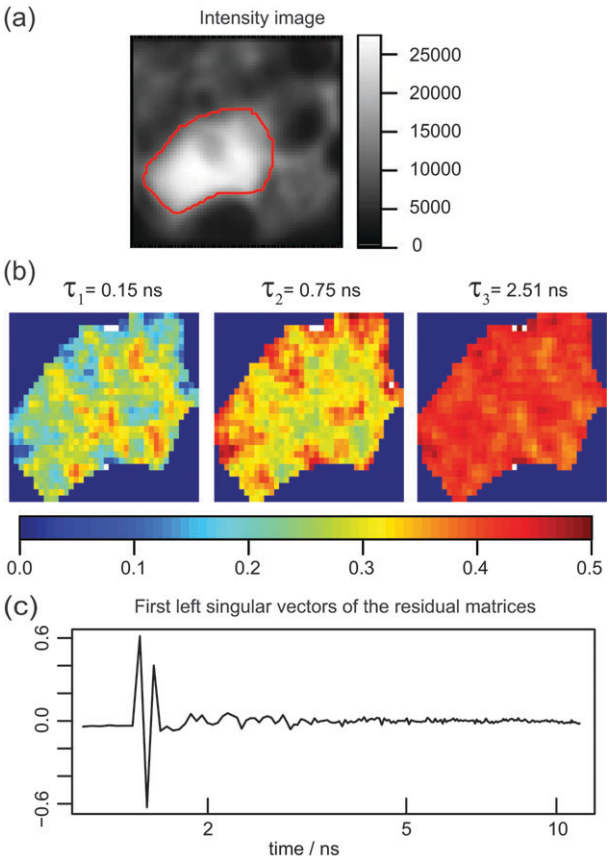

Fig. 3 Results of global analysis of a plant protoplast with expressed ECFP-L-EYFP. Detection at 465–495 nm (ECFP). (a) Intensity image, brightness of the pixels represents number of detected photons (64 × 64 pixels frame size, pixel size 235 nm), red contour indicates region selected for analysis, (b) spatial distributions of normalized amplitudes of components obtained from the analysis using a three-exponential model, (c) first left singular vector of the residual matrix.

the fluorescence lifetimes that correspond to the decay times of non-transferring donor molecules and of acceptor molecules were linked only between images measured at the same wavelength. Estimates of the fluorescence lifetimes that correspond to FRET and their amplitudes are summarized in Table 1.

Because of the presence of two transferring conformations of the ECFP chromophore with slightly different rate constants one can expect the presence of two different rise times of the acceptor fluorescence. However, given the limited signal to noise ratio and time resolution, two components in the rise part of the acceptor fluorescence cannot be resolved. Moreover, these two rise times get closer to each other at increasing transfer rates, making it impossible to resolve them separately.

The 2.51-ns component in the donor channel represents the population of non-interacting ECFP. The 0.75 ns component mainly represents an average lifetime of interacting ECFP molecules (but see also below), and can be used to calculate a transfer rate, taking also the average lifetime of 2.85 (2.37) ns for non-interacting ECFP calculated from a bi-exponential analysis using eqn (7) or (8), respectively. The calculated transfer rate constants using eqn (5) are 0.98 (0.91) ns^{-1}, which corresponds to an estimated distance between chromophores of 4.3 (4.1) nm, using R_0 = 4.9 nm.[11] The estimated distances in the case of ECFP-L-EYFP are in good agreement with the distance of 3.9 nm obtained by Evers *et al.*[37] from their macroscopic measurements and simulations for a linker of 23 amino acids. The definition of the length of the linker in their study is different from the one in our study. Their number of 23 corresponds to 12 in our case because the additional 11 amino acids are in fact part of the core of the proteins in our case. When the rise time is used that is obtained upon separately analyzing the acceptor channel, the calculated distance increases by only 1%. However, the global analysis leads to a reduction of the error margins for the estimated lifetimes. On the other hand, the distance calculated from the average donor lifetimes using definitions 7 or 8 lead to values of 5.9 nm and 5.8 nm, which is too long because of the influence of non-transferring donor molecules. The distances estimated using the various approaches are summarized in Table 2. It should be noted that the fitted decay time of 0.75 ns for the donor fluorescence is close to the 0.68-ns lifetime component that is observed for ECFP that is not linked to EYFP. The presence of some non-transferring ECFP might therefore contribute to the 0.75-ns lifetime. However, the fitted acceptor rise time was very similar, when global analysis included (0.75 ns) or not included (0.74 ns) the donor intensity decay. Therefore, the presence of non-transferring ECFP does not substantially influence the estimated transfer time.

EGFP-mCherry construct

The quantitative analysis of FLIM data is simplified considerably when donor molecules show mono-exponential fluorescence behavior in the absence of acceptor molecules, like is for instance the case for EGFP.[38] In order to check the fluorescence kinetics of EGFP in live cells, FLIM images of plant protoplasts transfected with only EGFP were analyzed. The fluorescence decay of EGFP molecules can well be described by a single exponential with a fluorescence lifetime of 2.45 ± 0.01 ns (results not shown). Global analysis of FLIM images of plant protoplasts transfected with EGFP-L-mCherry measured with the 525 nm band-pass filter (EGFP fluorescence detection window) are presented in Fig. 5. The analysis using a bi-exponential model results in fluorescence lifetimes of 0.48 ± 0.02 ns with an average contribution of 28% and 2.05 ± 0.03 ns with an average contribution of 72% (Fig. 5b, Table 3), resulting in an average fluorescence lifetime calculated with eqn (7) of $\langle\tau\rangle$ = 1.87 ns or $\langle\tau^*\rangle$ = 1.20 ns calculated with eqn (8). The lifetime of 2.05 ns is shorter than the unquenched lifetime of 2.45 ns and therefore the amplitudes of the short and long components cannot be directly ascribed to the fractions of interacting and non-interacting molecules. Both the high contribution (72%) and the shorter lifetime (2.05 ns) can be explained taking into account the presence of non-matured mCherry (NMmCherry). Maeder and co-workers used a similar construct in yeast and found that 50% of mCherry is not matured.[39] NMmCherry has similar spectroscopic properties as EGFP, but a shorter

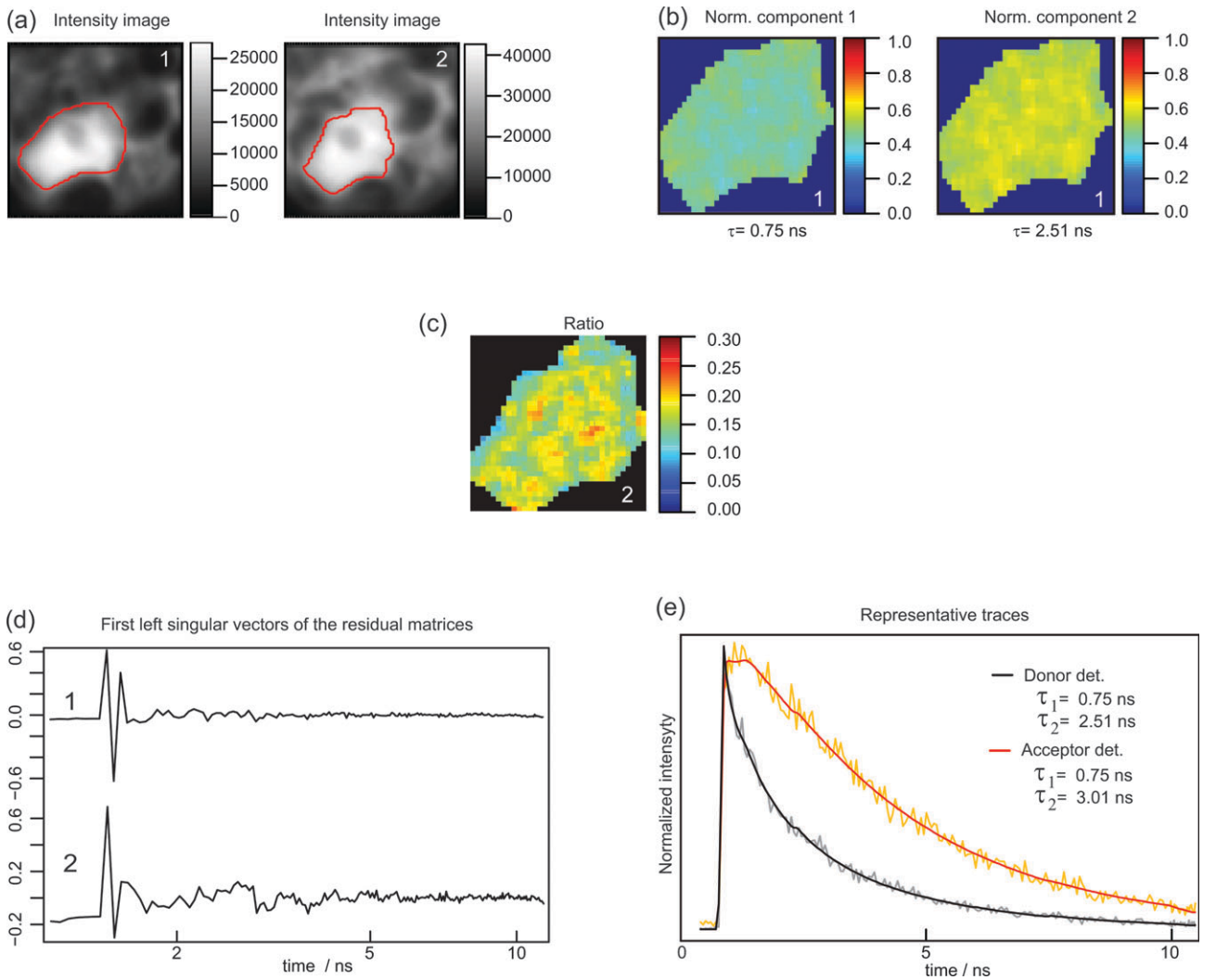

Fig. 4 Results of global analysis of plant protoplasts with expressed ECFP-L-EYFP. (a) Intensity images, brightness of the pixels represents number of detected photons (64 × 64 pixels frame size, pixel size 235 nm, 300–600 counts in the peak of the curve), red contour indicate regions selected for analysis (1-ECFP detection 469–495 nm, 2-EYFP detection 524–559 nm), (b) spatial distribution of fractional contributions of fluorescence components of ECFP obtained from a three-exponential fit excluding the component of 150 ps that represents auto-fluorescence, (c) spatial distribution of the absolute value of the ratio between the negative and positive amplitudes of the EYFP fast and slow kinetics components, respectively, (d) first left singular vectors of the residual matrices for the given cells; the fitting of the donor channel is somewhat better than that of the acceptor channel. (e) Representative traces and fit result for both detection channels.

Table 1 Estimates of fluorescence lifetimes after separate and simultaneous analysis of plant protoplasts containing ECFP linked to EYFP detected at two detection windows

	τ_1/ns	α_1 R[a]	τ_2/ns	α_2
Separate analysis of images from donor and acceptor detection channels[b]				
ECFP detection 469–495 nm	0.68 ± 0.02	0.27	3.04 ± 0.01	0.73
ECFP-L-EYFP detection 469–495 nm,	0.76 ± 0.03	0.44	2.51 ± 0.01	0.56
ECFP-L-EYFP detection 524–559 nm,	0.74 ± 0.10	0.20	3.01 ± 0.05	—
Global analysis of images from donor and acceptor detection channels[b]				
ECFP-L-EYFP detection 469–495 nm,	0.75 ± 0.02	0.44	2.51 ± 0.01	0.56
ECFP-L-EYFP detection 524–559 nm,	0.75 ± 0.02	0.20	3.01 ± 0.01	—

[a] R-absolute value of the ratio between negative and positive amplitudes estimated from analysis of the images from the acceptor detection channel. [b] Note that images from the donor detection window are analyzed with a 3-component analysis and that the component of 0.15 ns representing auto-fluorescence was excluded from further calculations.

Table 2 Estimated distances between ECFP and EYFP chromophores[a]

Calculation method	Calculated distance/nm
A	4.3 (4.1)
B	5.9 (5.8)
C	3.9

[a] The distance calculations are based on: (A) rise time of acceptor fluorescence (0.75 ns), (B) average donor lifetime in the presence and absence of acceptor, (C) distance observed by Evers *et al.*[37] for a linker length of 12 amino acids. The average donor lifetime is calculated using eqn (7), and the distances in parentheses are calculated when the average donor lifetime is calculated with eqn (8).

fluorescence lifetime.[9] It means that in the population of EGFP-L-NMmCherry molecules there is a mixture of directly excited NMmCherry and NMmCherry excited *via* resonance energy transfer from EGFP. Both components in the mixture emit fluorescence with a shorter lifetime than EGFP, which leads to the observed (average) lifetime of 2.05 ns.

FLIM images of the same plant protoplasts were also measured using a 590-nm band-pass filter to detect the rise of the acceptor fluorescence. The images were globally analyzed using a bi-exponential model. Analysis revealed the presence of a rise component of 0.58 ± 0.02 ns, reflecting energy transfer from EGFP to mCherry and a decay component of 2.010 ± 0.003 ns, which can mainly be attributed to mCherry. The rise time can be used for calculating the transfer rate (eqn (5)). The fluorescence lifetimes after separate analysis of the donor and acceptor detection windows are summarized in Table 3. A bi-exponential model was used for the simultaneous analysis of images obtained with both detection windows. The results are presented in Fig. 6. The fluorescence lifetime of the shortest component (attributed to the FRET process) was linked between images measured at both detection windows, while the lifetime of the long component was only linked between images detected within the same wavelength region. The analysis provides an estimate for the fluorescence lifetime of the short transfer component of 0.54 ± 0.01 ns. The longest lifetime is estimated to be 2.08 ± 0.01 ns for the donor channel and 2.03 ± 0.005 ns for the acceptor channel (Table 3).

The Förster radius R_0 for the FRET pair GFP-mCherry was calculated as described in ref. 40 as $R_0 = 0.0211(\kappa^2 n^{-4} Q_D \varepsilon_A J(\lambda))^{1/6}$ where $J(\lambda)$ is the overlap integral of the EGFP emission and mCherry absorption spectra, Q_D is the donor fluorescence quantum yield of EGFP in the absence of acceptor, which is taken to be $Q_D = 0.60$,[41] ε_A is the acceptor extinction coefficient at the absorbance maximum, which is taken to be $\varepsilon_A = 72\,000\ M^{-1}\ cm^{-1}$,[42] n is the refractive index of the medium which is taken to be $n = 1.34$, although this value is subject to some uncertainty[43] and κ^2 is the orientation factor, which is assumed to be $\frac{2}{3}$.[2] Based on these numbers, a value of $R_0 = 5.24$ nm is calculated, close to the value of 5.1 nm, which was recently reported by Albertazzi *et al.*[44] The distance r between the chromophores can now be calculated from eqn (6), using this value of $R_0 = 5.24$ nm and the transfer time of 0.54 ns. This leads to a distance of $r = 4.2$ nm. It is very important that the transfer time is being used for this

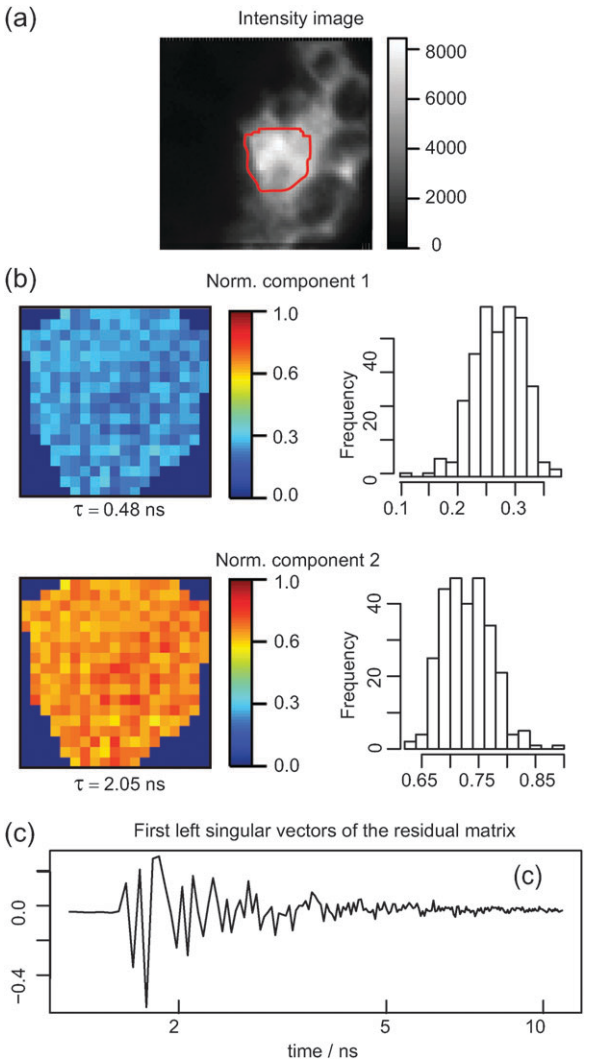

Fig. 5 Global analysis results of a representative image of a protoplast transfected with EGFP-L-mCherry detected with a 525 nm band-pass filter (EGFP). Global analysis was performed with a bi-exponential model. (a) Fluorescence intensity image (64 × 64 pixels frame size, pixel size 235 nm), red contour indicates the region that is analyzed, (b) spatial distribution and histogram of the fractional contributions of the components obtained from the fit using a bi-exponential model. (c) First left singular vector of residuals matrix, oscillates around zero, which indicates that the quality of the fit is good.

calculation. If one uses the average lifetime of the donor in the presence (1.87 ns) and absence (2.45 ns) of acceptor, one obtains a wrong distance of 6.4 nm or 5.2 nm depending which equation was used for calculating average lifetime.

Despite the fact that the linker is almost twice as long in the case of ECFP-L-EYFP as compared to the case of EGFP-L-mCherry, the estimated distances between the chromophores are almost identical being 4.3 nm and 4.2 nm, respectively. This can be explained by the fact that a flexible linker can give rise to a number of different conformations with different distances and orientations between the chromophores. Even in the case of very long linkers, conformations with short donor–acceptor distances can strongly contribute to the total fluorescence decay.[37]

Table 3 Estimates of fluorescence lifetimes after separate and simultaneous analysis of plant protoplasts containing EGFP linked to mCherry detected at two detection windows

	τ_1/ns	α_1 R[a]	τ_2/ns	α_2
Separate analysis of images from donor and acceptor detection channels				
EGFP	2.45 ± 0.01			
EGFP-L-mCherry det. 500–550 nm	0.48 ± 0.02	0.28	2.050 ± 0.003	0.72
EGFP-L-mCherry det. 585–615 nm	0.58 ± 0.02	0.25	2.010 ± 0.003	
Global analysis of images from donor and acceptor detection channels				
EGFP-L-mCherry det. 500–550 nm	0.54 ± 0.01	0.27	2.08 ± 0.01	0.73
EGFP-L-mCherry det. 585–615 nm	0.54 ± 0.0	0.25	2.030 ± 0.005	

[a] R-absolute value of the ratio between negative and positive amplitudes estimated from analysis of the images from the acceptor detection channel.

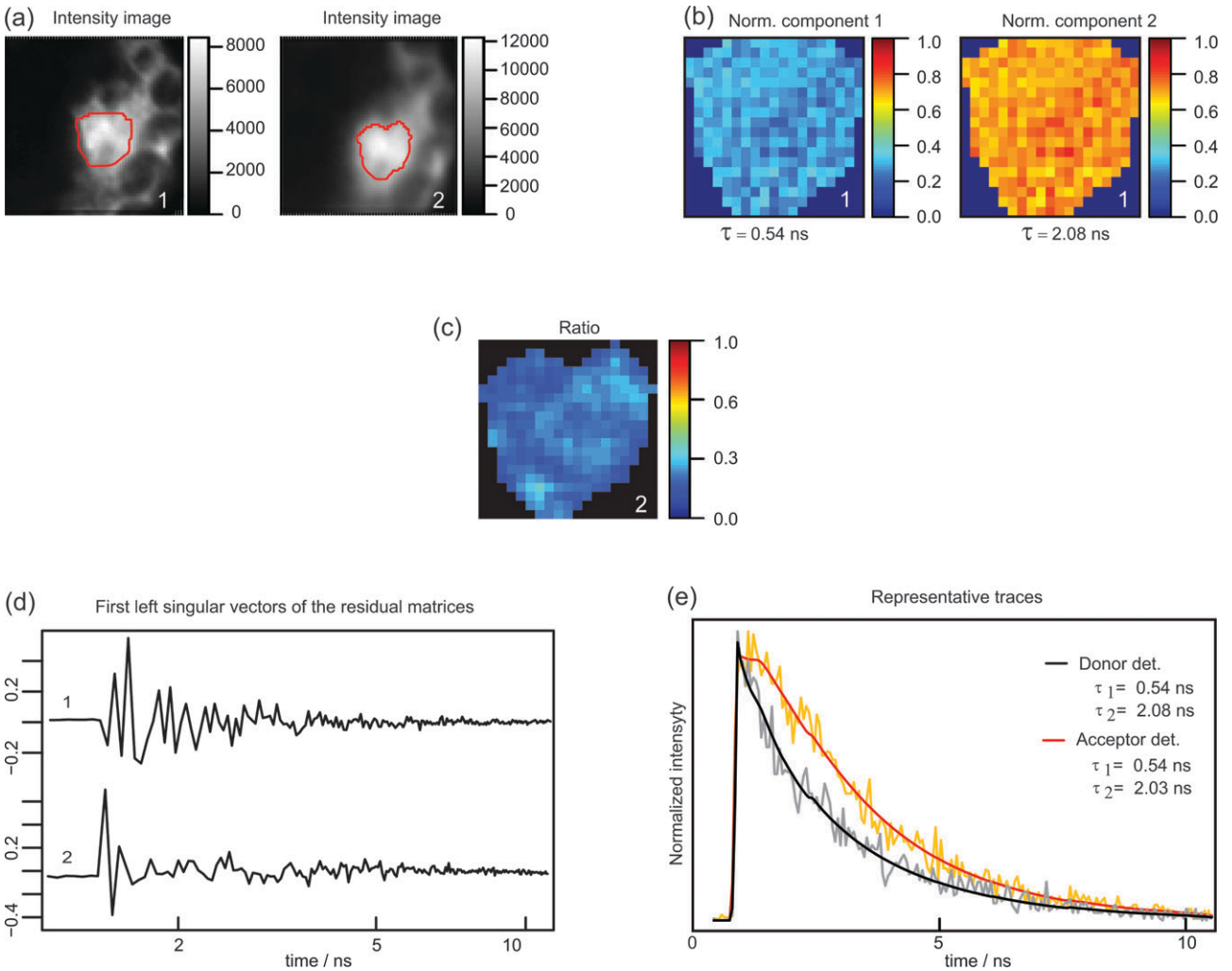

Fig. 6 Results of global analysis of plant protoplasts with expressed GFP linked to mCherry detected at two detection windows. (a) Intensity images (64 × 64 pixels frame size, pixel size 235 nm, 150–300 counts in the peak of the curve), red contours indicate the regions selected for analysis (1-EGFP 525 nm fluorescence detection, 2-mCherry 590 nm fluorescence detection), (b) spatial distribution of fractional contributions of fluorescence components of EGFP obtained from a bi-exponential fit, (c) spatial distribution of the absolute values of the ratio between the negative and positive amplitudes of the fast and slow components, respectively, detected at 600 nm, (d) first left singular vectors of the residuals for given cells, (e) representative traces and fit result for both detection channels.

Conclusions

A new methodology has been described for the detection of FRET in living cells. The method allows the accurate determination of the rate of FRET by globally (both spatially and spectrally) fitting the fluorescence kinetics of donor and acceptor molecules obtained in FLIM measurements. Combining the fitting of the fluorescence kinetics at different detection wavelengths allows to correct for the contribution of molecules that are not able to transfer their excitation energy

(for instance due to acceptor bleaching or incomplete maturation of visible protein), whereas the spatial global averaging leads to a substantial reduction of the error margins. In the case of EGFP-L-mCherry the distance between the chromophores is found to be 4.2 nm. In principle, this system is easier to study than the ECFP-L-EYFP construct because isolated EGFP shows a mono-exponential fluorescence decay curve in FLIM, whereas ECFP shows a bi-exponential decay. Nevertheless, an accurate distance determination could also be performed in the latter case, which yields a distance between the chromophores of 4.3 nm.

The main limiting factor for a proper analysis of the FLIM data is the signal-to-noise ratio, which at the moment can only be improved by increasing the measuring time. However, increasing the acquisition time is in most cases restricted by limited sample stability in live cells. Global analysis is advantageous since it increases the precision of the small number of estimated parameters that are obtained from all data.

Implementation

The data analysis procedures described in the previous sections have been implemented in the package **TIMP** for the "*R* project" for Statistical Computing. **TIMP** and *R* are freely available under the terms of the GNU General Public License.

Acknowledgements

This research was funded by the Sandwich Programme of Wageningen University, European Community (Marie Curie Research Training Network MRTN-CT-2005-019481 "From FLIM to FLIN") and Computational Science grant 635.000.014 from the Netherlands Organization for Scientific Research (NWO).

Notes and references

1 S. Pelet, M. Previte and P. T. C. So, *J. Biomed. Opt*., 2006, **11**(3), 1–11.
2 J. R. Lakowicz, *Principles of Fluorescence Spectroscopy*, Springer, New York, 3rd edn, 2006.
3 P. I. H. Bastiaens and A. Squire, *Trends Cell Biol*., 1999, **9**, 48–52.
4 B. van Oort, A. Amunts, J. W. Borst, A. van Hoek, N. Nelson, H. van Amerongen and R. Croce, *Biophys. J*., 2008, **95**, 5851–5861.
5 K. Broess, J. W. Borst and H. van Amerongen, *Photosynth. Res*., 2009, **100**, 89–96.
6 J. M. Beechem, *Methods Enzymol*., 1992, **210**, 37–54.
7 A. Bednarkiewicz and M. P. Whelan, *J. Biomed. Opt*., 2008, **13**(4), 1–13.
8 P. R. Barber, S. M. Ameer-Beg, J. D. Gilbey, R. J. Edens, I. Ezike and B. Vojnovic, *Proc. SPIE–Int. Soc. Opt. Eng*., 2005, **5700**, 171–181.
9 A. J. W. G. Visser, S. P. Laptenok, N. V. Visser, A. van Hoek, D. J. S. Birch, J. C. Brochon and J. W. Borst, *Eur. Biophys. J*., 2010, **39**, 241–253.
10 J. Wlodarczyk, A. Woehler, F. Kobe, E. Ponimaskin, A. Zeug and E. Neher, *Biophys. J*., 2008, **94**, 986–1000.
11 J. W. Borst, S. P. Laptenok, A. H. Westphal, R. Kühnemuth, H. Hornen, N. V. Visser, S. Kalinin, J. Aker, A. van Hoek, C. A. M. Seidel and A. J. W. G. Visser, *Biophys. J*., 2008, **95**, 5399–5411.
12 J. W. Borst, M. A. Hink, A. v. Hoek and A. J. W. G. Visser, *Proc. SPIE–Int. Soc. Opt. Eng*., 2003, **4963**, 231–238.
13 W. Becker, *Advanced Time-Correlated Single Photon Counting Techniques*, Springer, Berlin, 2005.
14 J. Aker, R. Hesselink, R. Engel, R. Karlova, J. W. Borst, A. J. W. G. Visser and S. C. de Vries, *Plant Physiol*., 2007, **145**, 339–350.
15 M. A. Hink, K. Shah, E. Russinova, S. C. de Vries and A. J. W. G. Visser, *Biophys. J*., 2008, **94**, 1052–1062.
16 T. Förster, *Zeitschrift für Naturforschung*, 1949, **4a**, 321–327.
17 N. Boens, M. Ameloot, I. Yamazaki and F. C. De Schryver, *Chem. Phys*., 1988, **121**, 73–86.
18 A. Grinvald and I. Z. Steinberg, *Anal. Biochem*., 1974, **59**, 583–598.
19 K. Vos, A. van Hoek and A. J. W. G. Visser, *Eur. J. Biochem*., 1987, **165**, 55–63.
20 R Development Core Team, *R*: *A language and environment for statistical computing*. R Foundation for Statistical Computing, Vienna, 2008.
21 N. Boens, N. Tamai, I. Yamazaki and T. Yamazaki, *Photochem. Photobiol*., 1990, **52**, 911–917.
22 J. Karolczak, D. Komar, J. Kubicki, T. Wrzowa, K. Dobek, B. Ciesielska and A. Maciejewski, *Chem. Phys. Lett*., 2001, **344**, 154–164.
23 P. J. Verveer, A. Squire and P. I. H. Bastiaens, *Biophys. J*., 2000, **78**, 2127–2137.
24 M. Maus, M. Cotlet, J. Hofkens, T. Gensch, F. C. De Schryver, J. Schaffer and C. A. M. Seidel, *Anal. Chem*., 2001, **73**, 2078–2086.
25 G. Golub and V. Pereyra, *Inverse Problems*, 2003, **19**, R1–R26.
26 G. H. Golub and V. Pereyra, *SIAM J. Numer. Anal*., 1973, **10**, 413–432.
27 S. Laptenok, K. M. Mullen, J. W. Borst, I. H. M. van Stokkum, V. V. Apanasovich and A. J. W. G. Visser, *Journal of Statistical Software*, 2007, **18**, 1–20.
28 G. H. Golub and C. F. v. Loan, *Matrix Computations*, Johns Hopkins University Press, 3rd edn, 1996.
29 W. D. Hoff, I. H. van Stokkum, H. J. van Ramesdonk, M. E. van Brederode, A. M. Brouwer, J. C. Fitch, T. E. Meyer, R. van Grondelle and K. J. Hellingwerf, *Biophys. J*., 1994, **67**, 1691–1705.
30 I. H. M. van Stokkum, D. S. Larsen and R. van Grondelle, *Biochim. Biophys. Acta, Bioenerg*., 2004, **1657**, 82–104.
31 J. W. Borst, M. A. Hink, A. van Hoek and A. J. W. G. Visser, *J. Fluoresc*., 2005, **15**, 153–160.
32 M. Tramier, I. Gautier, T. Piolot, S. Ravalet, K. Kemnitz, J. Coppey, C. Durieux, V. Mignotte and M. Coppey-Moisan, *Biophys. J*., 2002, **83**, 3570–3577.
33 K. M. Mullen, M. Vengris and I. H. Stokkum, *Journal of Global Optimization*, 2007, **38**, 201–213.
34 I. H. M. van Stokkum, *IEEE Trans. Instrum. Meas*., 1997, **46**, 764–768.
35 J. H. Bae, M. Rubini, G. Jung, G. Wiegand, M. H. J. Seifert, M. K. Azim, J.-S. Kim, A. Zumbusch, T. A. Holak, L. Moroder, R. Huber and N. Budisa, *J. Mol. Biol*., 2003, **328**, 1071–1081.
36 S. Ganesan, S. M. Ameer-Beg, T. T. Ng, B. Vojnovic and F. S. Wouters, *Proc. Natl. Acad. Sci. U. S. A*., 2006, **103**, 4089–4094.
37 T. H. Evers, E. M. W. M. van Dongen, A. C. Faesen, E. W. Meijer and M. Merkx, *Biochemistry*, 2006, **45**, 13183–13192.
38 M. Tramier, M. Zahid, J. C. Mevel, M. J. Masse and M. Coppey-Moisan, *Microsc. Res. Tech*., 2006, **69**, 933–939.
39 C. I. Maeder, M. A. Hink, A. Kinkhabwala, R. Mayr, P. I. H. Bastiaens and M. Knop, *Nat. Cell Biol*., 2007, **9**, 1319–1326.
40 M. A. Hink, N. V. Visser, J. W. Borst, A. van Hoek and A. J. W. G. Visser, *J. Fluoresc*., 2003, **13**, 185–188.
41 R. Y. Tsien, *Annu. Rev. Biochem*., 1998, **67**, 509–544.
42 N. C. Shaner, R. E. Campbell, P. A. Steinbach, B. N. G. Giepmans, A. E. Palmer and R. Y. Tsien, *Nat. Biotechnol*., 2004, **22**, 1567–1572.
43 R. S. Knox and H. van Amerongen, *J. Phys. Chem. B*, 2002, **106**, 5289–5293.
44 L. Albertazzi, D. Arosio, L. Marchetti, F. Ricci and F. Beltram, *Photochem. Photobiol*., 2009, **85**, 287–297.

